analytical chemistry

pubs.acs.org/ac Article

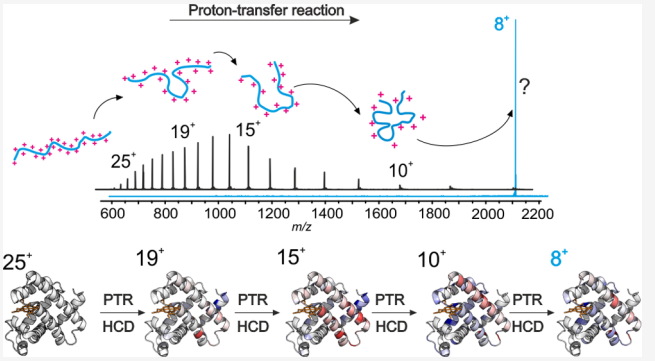
Proton-Transfer Reactions Modulate Protein Ion Structure to Yield Altered Backbone Cleavage Pathways in Top-Down Mass Spectrometry

Marek Polák, Lissa C. Anderson, Kristina Håkansson, Christopher L. Hendrickson, and Chad R. Weisbrod*

Cite This: *Anal. Chem.* 2026, 98, 29299−29311 Read Online

ACCESS | Metrics & More | Article Recommendations | Supporting Information

ABSTRACT: Proton-transfer reaction (PTR) has emerged as a powerful tool for top-down proteomics. It can mitigate spectral congestion and improve the signal-to-noise ratio of electrospray ionization (ESI)-generated intact proteins. We hypothesized that charge removal during PTR of Coulombically unfolded, denatured ESI ions induces rapid gas-phase isomerization and refolding, producing charge-state-dependent conformers with altered fragmentation behavior. Here, we test this hypothesis by systematically comparing fragmentation patterns of three model proteins, apomyoglobin, apocalmodulin, and histone H1, with and without PTR using high-resolution top-down mass spectrometry. Highly charged precursor ions were isolated, subjected to PTR, fragmented, and benchmarked against ions of the same charge state generated directly from ESI; ions generated under native-like conditions were also examined. Quantitative analysis of assigned fragment ions and $\log_2$ fold-change heatmaps reveal distinct fragmentation patterns, with some regions showing protection from fragmentation, while others yield newly observed or substantially enhanced fragment ions. Notably, characteristic fragmentation signatures around proline and aspartic acid residues further demonstrate structural differences. These results show that protein relaxation after PTR generates different gas-phase ion structures than are formed during ESI and explain, alongside mobile proton theory, why charge reduction produces different sets of fragment ions in top-down MS/MS, but can also yield fragmentation sites otherwise unavailable for higher-charged counterparts and the same charge states generated without PTR.



INTRODUCTION

In the past decades, proteomics has made significant strides in understanding relationships between protein structure and function.[1,2] Structural biology methods such as hydrogen−deuterium exchange (HDX), chemical cross-linking, native mass spectrometry, covalent and radical labeling, and ion mobility spectrometry have become widely adopted.[3−6] Considerable efforts have also been dedicated to improved ion activation methodology to enable near-complete sequence coverage and identification/localization of post-translational modifications (PTMs).[7−14] As a result, top-down proteomics has emerged as a powerful approach for analyzing proteoforms directly.

Despite its advantages, top-down proteomics faces several technological challenges. One major obstacle is the presence of heavy isotopes, which reduces the abundance of monoisotopic peaks, complicates accurate intact mass determination, and lowers signal-to-noise ratios (SNR) as ion current is dispersed among isotopologues.[15,16] A second obstacle arises during denaturing electrospray ionization (ESI), which generates broad distributions of multiply charged precursor and fragment ions, further complicating spectra and reducing SNR.[1]

Proton transfer reaction (PTR) reduces the charge states of multiply charged ions at a charge state dependent rate, thus spreading ion current across the available m/z range and reducing spectral congestion.[17−20] However, excessive charge reduction can cause analyte ions to fall outside the detectable m/z range or become neutralized, leading to signal loss.

To address this limitation, the McLuckey group developed parallel ion parking to selectively control charge reduction rates.[21,22] As a result, analytes are concentrated into a single charge state or narrow charge state distribution which significantly increases their SNR, often by an order of

Received: June 10, 2026
Revised: September 4, 2026
Accepted: September 14, 2026
Published: September 28, 2026



ACS Publications © 2026 The Authors. Published by American Chemical Society

https://doi.org/10.1021/acs.analchem.6c04013
Anal. Chem. 2026, 98, 29299−29311

Downloaded from pubs.acs.org/ancham/article-pdf/98/40/29299/6868094/acs.analchem.6c04013.pdf by FLORIDA STATE UNIV user on 02 November 2026

magnitude or greater.[23] PTR is commercially available on some Fourier transform mass spectrometry (FTMS) instruments, and specialized instrument modifications have enabled parallel ion parking in increasingly complex applications,[24,25] including successful operation on a 21 T (T) Fourier-transform ion cyclotron resonance (FT-ICR) mass spectrometer.[23]

In a previous study,[23] PTR and parallel ion parking were applied to denatured apomyoglobin ions, which were selectively parked into charge states ranging from $[M + 14H]^{14+}$ to $[M + 9H]^{9+}$. Subsequent collision-induced dissociation (CID) tandem mass spectrometry (MS/MS) revealed distinct fragmentation patterns and different sequence coverage compared to nonparked ions across these charge states. These differences were attributed to gas-phase structural rearrangements induced by charge reduction.[26] Building on these findings, the aim of the current study is to explore the gas-phase structures of intact proteins by comparing fragmentation behavior of ions generated by ESI directly with the same charge states produced through PTR using high-resolution top-down mass spectrometry (MS).

Highly charged protein ions introduced under denaturing ESI conditions are expected to adopt linear-like conformations in the gas-phase.[27] As protons are removed via PTR, decreased Coulomb repulsion initiates gas-phase structural rearrangements,[28] which may expose previously inaccessible regions of the protein and produce unique fragment ions.

To test this hypothesis, we studied three proteins: apomyoglobin, apocalmodulin and histone H1. These model proteins were selected for amino acid composition and pK_a. Highly charged precursors were isolated and subjected to PTR, followed by MS/MS analysis of the charge-reduced product ions. These charge-reduced precursors were compared to their counterparts generated directly from denaturing ESI, as well as ions generated under native-like conditions. Fragment ions matched to the sequence were quantified, and the resulting data demonstrate distinct fragmentation patterns, indicating that gas-phase structures depend on the method of charge state generation (PTR vs no PTR). Moreover, some regions experienced a loss of fragment ions while other regions gained newly observed fragments, presumably because of extensive proton removal and gas-phase refolding. Observed fragmentation behavior confirms and extends previous work demonstrating that PTR-induced charge reduction can significantly alter structural outcomes.[28−30] Exploitation of these observations may lead to improved sequence coverage or "targeted" sequence coverage in specific protein regions with low fragmentation efficiency.

EXPERIMENTAL SECTION

Materials and Chemicals

Protein standards: apomyoglobin (Cat. number A8673) from equine skeletal muscle and recombinant bovine calmodulin (Cat. number C4874) were obtained from MilliporeSigma (St. Louis, MO, USA). Recombinant human histone H1 (UniProt entry P07305) was purchased from BPS Bioscience (Cat. number 54043; San Diego, CA, USA). Unless stated otherwise, all solvents were purchased from Honeywell Burdick & Jackson (Charlotte, NC, USA) in LC-MS grade. For apomyoglobin and calmodulin, lyophilized powders were dissolved in 10 mM ammonium acetate (MilliporeSigma) to prepare a 200 μM stock solution, then diluted with the same buffer to a final protein concentration of ∼5 μM for native-MS experiments. For denaturing experiments, 5 μg of each protein were transferred into a new Eppendorf tube and diluted into 50% methanol (MeOH) and 0.1% formic acid (FA, Thermo Fisher Scientific, Waltham, MA, USA) in water (v/v), then sprayed as 1−2 μM. Histone H1 lyophilized powder (100 μg) was reconstituted in 10 mM ammonium acetate at 1 mg/mL to obtain a stock solution. For denaturing experiments, a 10 μg sample was desalted using a C18 column (Optimize Technologies, Oregon City, Oregon, USA) with 0.1% FA, eluted with 80% acetonitrile containing 0.1% FA, then diluted into 50% MeOH with 0.1% FA and sprayed as 1−2 μM. For native MS experiments, 10 μg of histone H1 was desalted using Amicon Ultra centrifugal filter units with a 10 kDa molecular weight cutoff (MilliporeSigma) following manufacturer's protocol. The protein was subsequently diluted with 10 mM ammonium acetate to a concentration of ∼5 μM prior to analysis.

Experimental Workflow

Samples were ionized by nanoflow-ESI (NSI) using a fused silica capillary with I.D. of 25 μm. The NSI source was adopted from the University of Washington Proteomics Resource design (https://proteomicsresource.washington.edu/protocols05/nsisource.php). The capillary was connected through a high-voltage union to the ESI power supply and to a syringe pump operating at 1 μL/min and 2 μL/min for denaturing and native experiments, respectively. The applied ESI spray voltage varied between 2.75 kV and 3.0 kV, and the inlet capillary temperature was set to 300 °C. All experiments were performed on an Orbitrap Eclipse Tribrid (Thermo Fisher Scientific, San Jose, CA, USA) instrument[31] equipped with an EASY-IC and proton-transfer charge reduction capabilities. All spectra were acquired using the Orbitrap mass analyzer at a resolving power of 240,000 at m/z 200. Data were acquired in positive ion mode with a scan range of m/z 200−4000 (high-mass range mode). For MS^1 experiments, 20 transients were summed, and then 10 scans were collected. For MS^n experiments, 100 transients were summed and 10 spectra collected.

First, we acquired MS^1 spectra of the denatured protein samples to obtain broadband m/z information. The highest observable charge state for each protein was quadrupole isolated ($[M + 25H]^{25+}$ for apomyoglobin, $[M + 23H]^{23+}$ for apocalmodulin, and $[M + 38H]^{38+}$ for histone H1) with a 2−3 Da isolation window and transferred to the linear RF ion trap (IT) for PTR. PTR reaction times were modulated to maximize SNR of the desired reduced charge state. The precursor automatic gain control (AGC) target was set to 1000% (5×10^5 charges) to maintain sufficient ion population for downstream fragmentation. Following PTR (MS^2), the desired charge-reduced product ion was isolated in the ion trap for MS^3 analysis using a 5 Da isolation window. SNRs were calculated from isolation-only PTR-MS^3 experiments (i.e., without subsequent activation). Each PTR-generated precursor ion was then fragmented using higher-energy collisional dissociation HCD, resonant CID, electron-transfer dissociation (ETD), or EThcD. Both CID and HCD energies typically ranged from 35 to 60% normalized collision energy (NCE) and were tuned for each charge state to optimize fragmentation efficiency. ETD reaction times ranged from 3 to 8 ms, and supplemental HCD activation (∼40% NCE) was applied when needed to increase the fragment ion yield for lower charge states.[12] Specific PTR/ETD reaction times and collision energies are included in the Supporting Information in Supplemental Table S1.

For comparison, MS^2 experiments were also performed on the corresponding charge states generated directly by ESI, without applying PTR. These precursor ions were isolated in the ion trap, and their SNR values were calculated from isolation-only MS^2 scans (i.e., no fragmentation); AGC targets were then adjusted to match ion populations between the "no PTR" (MS^2) and "PTR-reduced" (MS^3) precursor ion charge states. Fragmentation conditions were matched to the MS^3 conditions used for PTR-generated ions, and 100 transients were averaged for each spectrum. All fragmentation spectra were acquired in technical triplicate.

Data Analysis

Raw spectra were averaged within Freestyle software (Thermo Fisher Scientific) and exported as profile-mode.txt files, which contain m/z and abundance pairs (x-y plot format). ExD Viewer[7] software was used for fragment ion assignment. Each spectrum was searched

Downloaded from pubs.acs.org/ancham/article-pdf/98/40/29299/6880948/acs.analchem.6c04013.pdf by FLORIDA STATE UNIV user on 02 November 2026

https://doi.org/10.1021/acs.analchem.6c04013
Anal. Chem. 2026, 98, 29299−29311

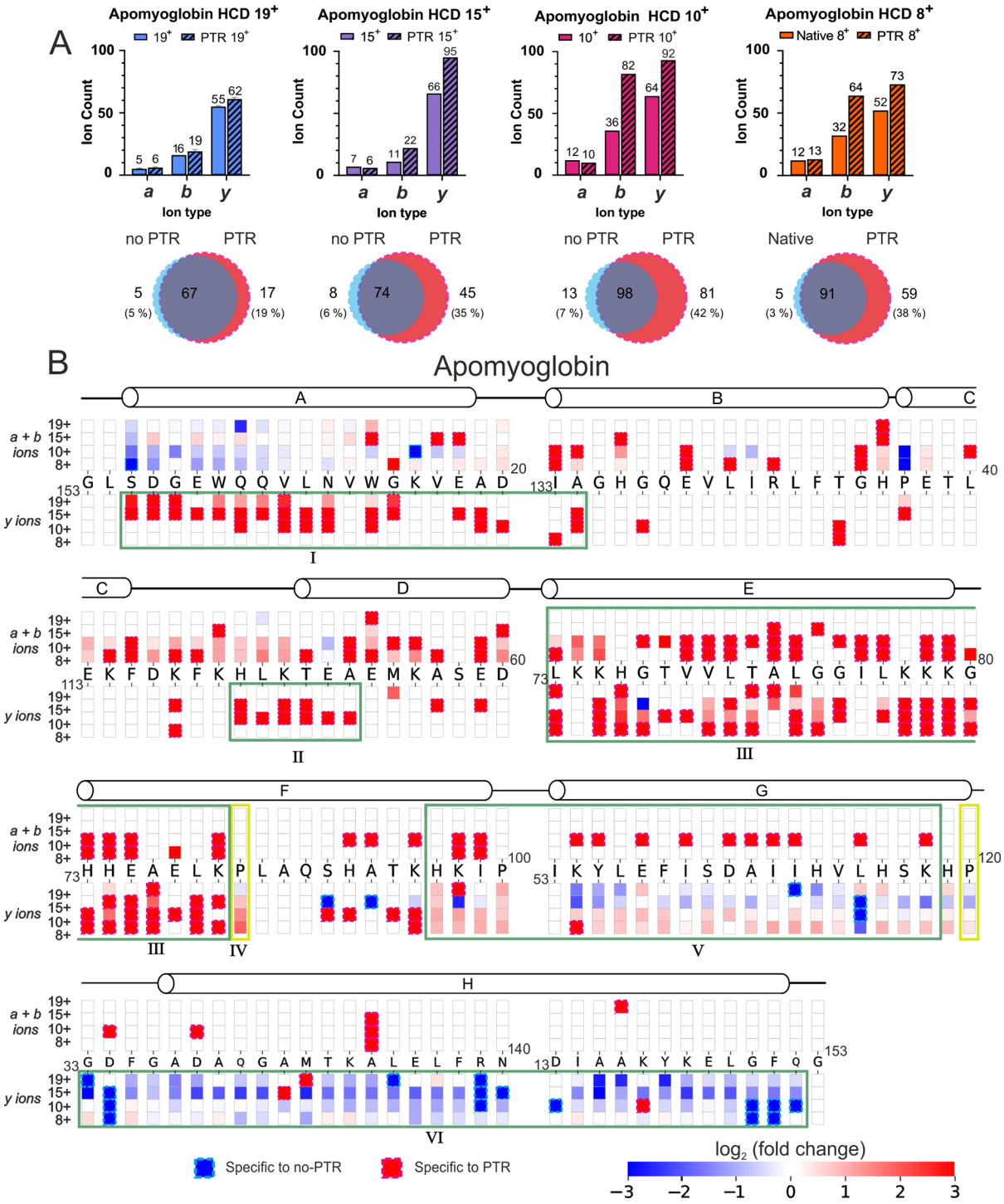


Figure 1. (A) Bar plots depict the number of assigned fragment ions from apomyoglobin for different charge states, generated with or without PTR, using HCD. The Venn diagrams below each bar plot contain the number of fragment ions that are unique to PTR, unique to no PTR, and common to both methods, for each charge state. (B) Heatmap of apomyoglobin showing the $\log_2$ fold change of fragment ion abundance with and without PTR. The amino acid sequence of myoglobin is shown in the middle, with the protein secondary structure indicated above the heatmap. The squares represent the specific fragment ions observed at each interresidue cleavage site: *a*/*b*-type fragment ions are above the sequence, and *y*-type fragments are displayed below the sequence. Each row represents a precursor ion charge state. Red squares indicate increased fragment ion abundance relative to no PTR, and blue squares indicate decreased fragment ion abundance relative to no PTR. Fragment ions that were uniquely generated either with or without PTR are indicated with blue or red dashed box outlines, as indicated by Venn diagrams.

against the corresponding protein sequence with a fragment mass tolerance of ±10 ppm. Recalibration was enabled and applied based on high-confidence fragment ion assignments, with the baseline filter disabled to ensure preservation of low-abundance ions. Several parameters were adjusted relative to software default settings to improve assignment accuracy: the peak-picking SNR threshold was set to 3, the maximum allowable charge state was constrained to match the precursor ion charge state, and ion-type priorities were set such that canonical fragment ions were evaluated first, followed by neutral-losses, and finally side-chain cleavage products. Spectra were

https://doi.org/10.1021/acs.analchem.6c04013
Anal. Chem. 2026, 98, 29299−29311

Downloaded from pubs.acs.org/ancham/article-pdf/98/40/29299/6880948/acs.analchem.6c04013.pdf by FLORIDA STATE UNIV user on 02 November 2026

searched for single and double neutral losses ($-H_2O$, $-NH_3$) in collisional activation MS/MS data (CID and HCD). Internal fragment ions were not considered. For CID and HCD spectra, *a*-, *b*- and *y*- ion series were queried. For ETD spectra, c'-, $z^\bullet$-, $a^\bullet$- and y'-fragment ion series were queried, with one hydrogen rearrangement (±H) allowed.

All fragment ion assignments were subsequently manually reviewed, and any ions with questionable assignments or ion scores below 1 were removed. Spectra were deconvolved to neutral, monoisotopic mass in ExDViewer, and the abundance of each fragment ion was extracted. These abundances were normalized to the total ion current (TIC) of the corresponding averaged spectrum prior to quantitative comparison. The resulting TIC-normalized values were used to calculate the $\log_2$ fold-change ($\log_2$FC) for each fragment ion according to eq 1:

$$Log_2FC = log_2\left(\frac{Fragment\ ion_{PTR} + \Delta}{Fragment\ ion_{noPTR} + \Delta}\right) \quad (1)$$

A small pseudocount ($\Delta \approx 1 \times 10^{-13}$), corresponding to one millionth of the lowest fragment ion abundance in the data set, was added to accommodate missing values and avoid undefined log(0) terms. A Python script was used to generate fragment-ion heatmaps displaying the $\log_2$FC values shown in this manuscript. Pseudocount can produce extreme $\log_2$FC values for fragment ions unique to experimental conditions, therefore, visualization required a nonlinear color scale for enhanced sensitivity. Only the linear region around zero, representing >90% of all quantified fragments, was used for heatmap visualization (range indicated by the gray dashed lines in Supplemental Figure S1). Fragment ions present exclusively in either the PTR or no-PTR condition were plotted separately and are indicated in the heatmaps with blue or red dashed borders. For heatmap visualization into X-ray structural models, a custom Python script was used with PyMOL software (v. 3.1.6.1; Schrödinger LLC, New York, NY).

RESULTS AND DISCUSSION

PTR has demonstrated strong utility in addressing key challenges encountered in top-down proteomics, especially spectral congestion and low SNR of both precursor and fragment ions.[23,24,32−34] Previous experiments with intact apomyoglobin showed that CID fragmentation of charge-reduced precursor ions can increase sequence coverage compared to the same charge state generated directly from denaturing ESI.[23] This observation led to the hypothesis that structural changes induced by PTR, specifically gas-phase rearrangements that occur as Coulomb repulsion decreases through successive rounds of charge reduction, may influence fragmentation behavior.[28] Such rearrangements could expose new cleavage sites or alter the availability of mobile protons, which affect backbone dissociation pathways.[35−38] In this study, we systematically tested this hypothesis by examining apomyoglobin, apocalmodulin, and histone H1 across multiple charge states and fragmentation conditions.

Apomyoglobin

Apomyoglobin (17 kDa) was electrosprayed from a denaturing solution, and one of the highest observable charge states, $[M+25H]^{25+}$, was isolated and subjected to PTR, and reduced to $25^{+\xrightarrow{PTR}}19^+$ ($^{PTR}19^+$), $25^{+\xrightarrow{PTR}}15+$ ($^{PTR}15^+$), and $25^{+\xrightarrow{PTR}}10^+$ ($^{PTR}10^+$), and $25^{+\xrightarrow{PTR}}8^+$ ($^{PTR}8^+$). (Supplemental Figure S2). Reduced precursors were individually isolated and fragmented by HCD, ETD, and resonant CID. Each reduced charge state was compared directly to the corresponding one generated directly from ESI without PTR (no PTR) under identical experimental conditions. The most extensively reduced precursor, $25^{+\xrightarrow{PTR}}8^+$, was also compared to the $[M + 8H]^{8+}$ charge state of apomyoglobin electrosprayed under native-like conditions to evaluate similarities and differences in gas-phase structure across all conditions (Supplemental Figure S3).

Figure 1 and Supplemental Figure S4 and S5 summarize the results, showing the number and types of assigned fragment ions across all precursor ion charge states for apomyoglobin with and without PTR. Figure 1A displays bar plots for HCD fragmentation, and the accompanying Venn diagrams highlight fragment ions unique to each condition (no PTR vs PTR). These Venn diagrams show a consistent trend with unique fragment ions appearing both with and without PTR. In Figure 1A, the HCD fragmentation of the PTR-generated charge states shows a general increase of assigned fragment ions with progressive PTR.

The only exception occurs for the $^{PTR}8^+$, which shows an overall decrease in the number of all assigned fragments compared to $^{PTR}10^+$ (Supplemental Figure S3). This decrease is likely related to the lower number of mobile protons. Overall, 17, 45, 81, and 59 fragment ions unique to the PTR condition were observed for $^{PTR}19^+$, $^{PTR}15^+$, $^{PTR}10^+$ and $^{PTR}8^+$, respectively.

The aforementioned experimental approach was also applied with ETD[39] (Supplemental Figure S4A). ETD spectra were searched for $a^\bullet$, y', c' and $z^\bullet$ fragments[40] (Zubarev nomenclature), with *b*-type fragments additionally considered in EThcD mass spectra. We expected that PTR-induced structural rearrangements would alter the ETD fragmentation pattern, producing differences in which c' and $z^\bullet$ backbone cleavages were observed. As shown in Supplemental Figure S4A, higher charge PTR-generated precursor ions, $^{PTR}19^+$, and $^{PTR}15^+$, yielded 20 and 18 new unique fragment ions, respectively. PTR charge reduction to lower charge states coupled with supplemental activation following ETD (EThcD) provided higher numbers of unique fragment ions; 47 and 79 new fragment ions observed for $^{PTR}10^+$ and $^{PTR}8^+$ charge states, respectively. Although fragmentation of $^{PTR}8^+$ produced 79 unique fragment ions, only 12 and 19 were assigned as c'- and $z^\bullet$-types. While the goal of supplemental activation[12] is to liberate nondissociated ETD (ETnoD) products, many new *b*- and *y*-type ions also arise as byproducts (Supplemental Figure S4B). Electron-based fragmentation has been used to provide relevant structural information,[41−43] however, ETD/EThcD provided only limited additional structural information in this context. Here, the preferred cleavage sites we observed align with published studies,[36,37,44] including abundant cleavages at Arg, Phe, Asn, or Gly residues, as well as collisional cleavages from the C-terminal side of aspartic acid when supplemental activation is applied (Supplemental Figure S4B).[45,46]

Resonant CID was also used to determine how PTR-induced charge reduction influences fragmentation under slow-heating conditions. As shown in Supplemental Figure S5A, the number of unique assigned fragment ions increases relative to their no-PTR couterparts at the $^{PTR}15^+$ charge state (14, 33, and 20 for $^{PTR}19^+$, $^{PTR}15^+$ and $^{PTR}10^+$, respectively) (see Venn diagrams in Supplemental Figure S5A; Figure 1A). Unlike HCD, which generated more unique fragments, CID of $^{PTR}8^+$ yielded only 16 unique fragment ions—failing to produce any additional fragment assignments over native-like 8+. Again, this observation may be explained by the decreased number of mobile protons, which limits the observable fragmentation sites. Resonant CID is a slow-heating process that takes place

Downloaded from pubs.acs.org/ancham/article-pdf/98/40/29299/6868948/acs.analchem.6c04013.pdf by FLORIDA STATE UNIV user on 02 November 2026

https://doi.org/10.1021/acs.analchem.6c04013
Anal. Chem. 2026, 98, 29299−29311

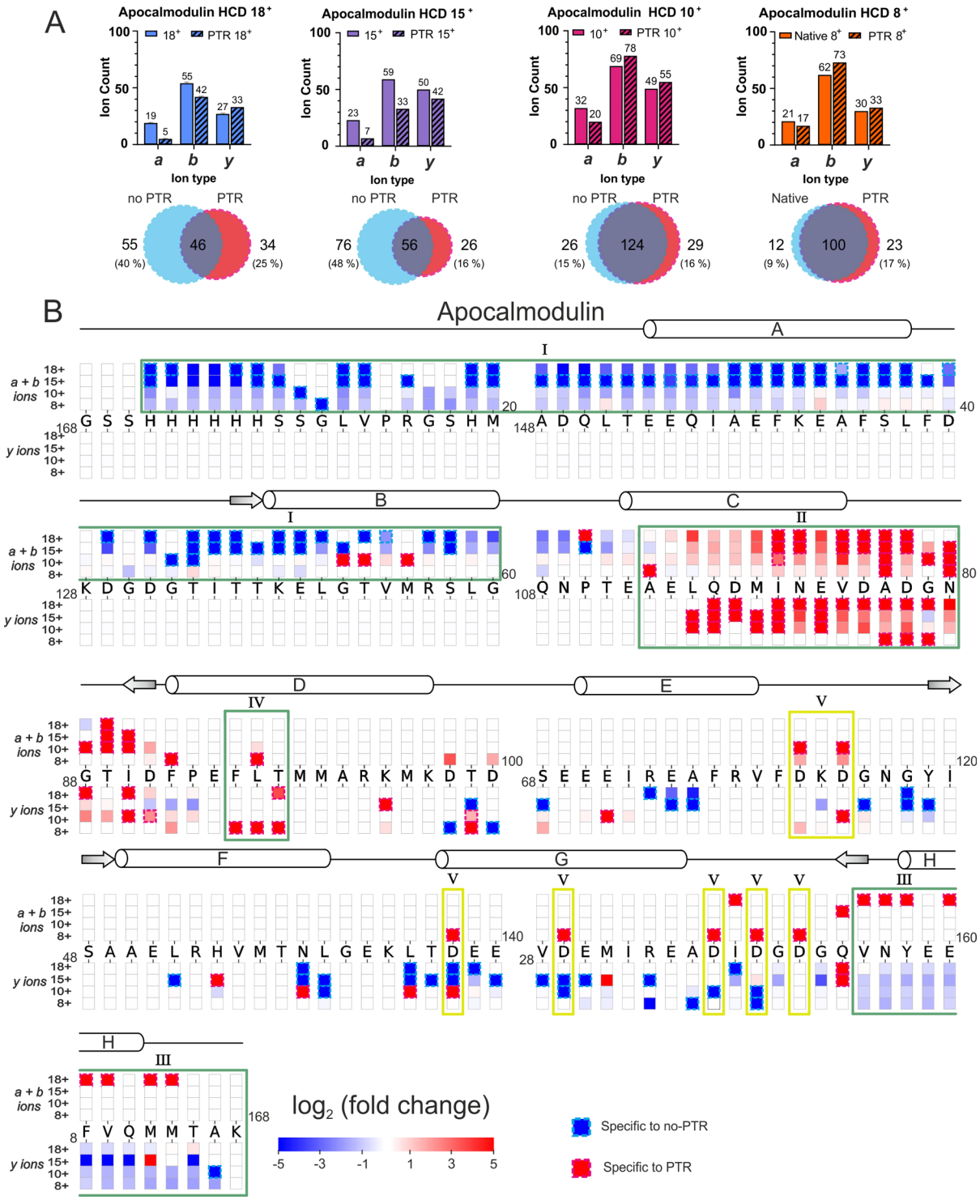


Figure 2. (A) Bar plots depict the number of assigned HCD fragment ions from apocalmodulin for different precursor ion charge states, generated with and without PTR. The Venn diagrams below each bar plot show the number of fragment ions unique to each condition. (B) Heatmap of apocalmodulin showing the $\log_2$ fold change in fragment-ion abundance with and without PTR. The amino acid sequence is shown in the middle, with protein secondary structure indicated above the heatmap. The small squares represent fragment ions observed at each interresidue cleavage site: *a*/*b*-ions are displayed above the sequence; *y*-ions are displayed below the sequence. Each row corresponds to a precursor ion charge state. Red squares indicate increased fragment ion abundance relative to no PTR, and blue squares indicate decreased fragment ion abundance relative to no PTR. Fragment ions observed exclusively with or without PTR are outlined with red or blue dashed boxes respectively, as indicated by Venn diagrams.

over milliseconds.[47,48] This timescale could allow any gas-phase rearrangement introduced by PTR to be partially or fully undone prior to fragmentation,[49−51] which then produces fragmentation patterns similar to the same charge state counterpart generated directly from ESI. We also tested a shorter resonant CID activation time (1 ms) to evaluate

https://doi.org/10.1021/acs.analchem.6c04013
Anal. Chem. 2026, 98, 29299−29311

Downloaded from pubs.acs.org/ancham/article-pdf/98/40/29299/6868094/acs.analchem.6c04013.pdf by FLORIDA STATE UNIV user on 02 November 2026

whether minimizing slow heating would better preserve PTR-induced structural ion conformations; however, these results were similar to the standard 10 ms activation (Supplemental Figure S5B).

The number of assigned fragment ions is informative; however, it does not capture changes in fragment-ion abundance. To better assess and visualize these differences, we quantified all assigned fragment ions and generated heatmap. The detailed HCD heatmap for apomyoglobin is shown in Figure 1B. The heatmap depicts the protein sequence and it's secondary structure, with colored tiles positioned above/below the sequence to indicate specific fragment-ion observations at the quantitative level. N-terminal ions (*a*- and *b*-ions combined) are displayed above the sequence, and *y*-ions are shown below the sequence. Each row corresponds to $\log_2$FC difference in fragment ion abundance between PTR and the same non reduced, ESI-generated precursor. Similar to heatmaps used to visualize HDX data, red squares indicate fragment ions that increased in abundance with PTR, whereas blue squares indicate decreased abundance or fragment ions that were no longer observed. Unique fragment ions as represented by Venn diagrams are outlined in the heatmap as tiles with red or blue dashed borders.

PTR produced several notable changes in fragmentation pattern across the protein (Figure 1B). Within helix A, small *b*-ions were generated to a lesser extent following PTR, whereas a new series of large *y*-ions (S3-A22; y_{132}−y_{151}, region I highlighted in a green box) appeared predominantly in $^{PTR}19^+$ and $^{PTR}15^+$ spectra. The small *b* fragments complementary to these larger *y*-ions were often not detected, or showed low abundance, likely reflecting PTR-induced changes in mobile proton distribution. Upon further charge reduction, the number of newly generated fragment ions decreased, and these larger *y*-ions were no longer detected in the $^{PTR}8^+$ charge state.

Additional changes were observed in the intervening loop and helix D (region II). Although fewer *b*- or *y*-ions are observed in the $^{PTR}19^+$ state, a distinct set of new *y*-ions spanning residues H48−A53 (y_{101}−y_{106}; region II) emerged, accompanied by increased *b* ion abundance across E41-D60. These trends indicate that PTR-induced rearrangement alters the susceptibility of helix D to fragmentation. The most pronounced changes occurred in helix E and the N-terminal region of helix F (L61−K87, region III), where a consistent series of unique fragment ions appeared across the reduced charge states. Apparently, this region was especially exposed following PTR. A representative example (fragment ion b_{71}) is illustrated in Supplemental Figure S6.

Proline's structural rigidity can influence local fragmentation behavior because its cyclic side chain restricts backbone flexibility. Although proline residues can exist in either *cis*- or *trans*- peptide-bond conformations, gas-phase *cis*-/*trans*-isomerization is unlikely under typical MS conditions and is easily converted by ion activation.[52,53] Therefore, the fragmentation differences observed here are more plausibly attributed to PTR-induced structural rearrangements rather than bond isomerization. This effect is apparent at residue P88 in helix F (region IV, yellow box in Figure 1B). The y_{66} ion, generated by cleavage N-terminal to P88, is less abundant in the $^{PTR}19^+$ spectrum but becomes more prominent with further charge reduction. Interestingly, a similar pattern is observed at P120, but not at P100. These site-specific differences suggest that PTR-driven changes in charge distribution and local structure can modulate how proline residues influence backbone accessibility and the resulting fragmentation pattern.

A distinct fragmentation behavior was also observed for helices G and H at the C-terminus, both of which are predominantly covered by lower molecular weight (MW) *y*-ions. In helix G (region V), these *y*-ions were decreased in abundance in the $^{PTR}19^+$ and $^{PTR}15^+$ states compared to the no PTR controls. However, this trend reversed with more extensive charge reduction, in the $^{PTR}10^+$ state, new *b*-fragment ions from helix G were detected. This observation indicates that, with PTR, the accessibility of this region is altered. When $^{PTR}8^+$ was compared to the native-like 8^+ charge state, the fragmentation pattern differed markedly, suggesting that extensive charge reduction produces a structure (or structures) that are not equivalent to the electrospray-generated native-like conformation. In contrast, the intervening loop and the C-terminal helix H (region VI) produced fewer *y*-fragment ions after PTR, suggesting this region becomes less accessible to fragmentation. These observations are consistent with those from the Brodbelt group,[37] which also reported a rich cluster of small *b*- and *y*- ions at the termini, but overall decreased fragmentation at low charge states.

The Konermann group employed molecular dynamics (MD) simulations to investigate the gas-phase structure of unfolded and Coulombically stretched ubiquitin gaseous ions,[28] and reported that the driving force in gas-phase structural rearrangement is the electrostatic interaction of charged amino acid side-chains, specifically D, E, K, and R residues. Thus, we selected apocalmodulin (18 kDa) and histone H1 (22 kDa) for further study because they contain high numbers of these residues. These two proteins provide useful test cases for assessing how amino acid residue composition influences gas-phase behavior following PTR.

Apocalmodulin

Calmodulin is an acidic protein (estimated pI 4.31) and contains 17 × D, 21 × E, 8 × K, and 7 × R residues. Here, the $[M + 23H]^{23+}$ precursor ion of apocalmodulin was isolated and then stepwise reduced to $^{PTR}18^+$, $^{PTR}15^+$, $^{PTR}10^+$ and $^{PTR}8^+$ charge states, followed by HCD fragmentation (Supplemental Figure S7). The $^{PTR}8^+$ HCD MS/MS spectrum was compared with the HCD spectrum obtained from native-like $[M + 8H]^{8+}$ apocalmodulin precursor ions generated by electrospray from an ammonium acetate solution. As shown in Figure 2A, the total number of fragment ions matched to the sequence increased with progressive charge reduction from $^{PTR}18^+$ to $^{PTR}10^+$ (80, 82, and 153 total fragment ions for $^{PTR}18^+$, $^{PTR}15^+$ and $^{PTR}10^+$, respectively; see Venn diagrams in Figure 2A). However, the overall fragment count masks substantial changes in fragmentation behavior. Many fragment ions observed for the corresponding no-PTR precursor ions were absent after PTR (55 and 76 ions for $^{PTR}18^+$ and $^{PTR}15^+$, respectively), while new fragment ions appeared. Manual inspection showed that small N-terminal b-ions were frequently reduced in abundance or absent after PTR, indicating substantial redistribution of fragmentation pathways. Consequently, similar fragment-ion counts can still correspond to substantially different fragmentation patterns. Although the differences between $^{PTR}18^+$ and $^{PTR}15^+$ are relatively modest, substantially larger changes are observed for $^{PTR}10^+$. This trend may reflect the changing balance between proton mobility and charge localization as charge is progressively reduced. At higher charge

Downloaded from pubs.acs.org/anchem/article-pdf/98/40/29299/6880948/acs.analchem.6c04013.pdf by FLORIDA STATE UNIV user on 02 November 2026

https://doi.org/10.1021/acs.analchem.6c04013
Anal. Chem. 2026, 98, 29299−29311

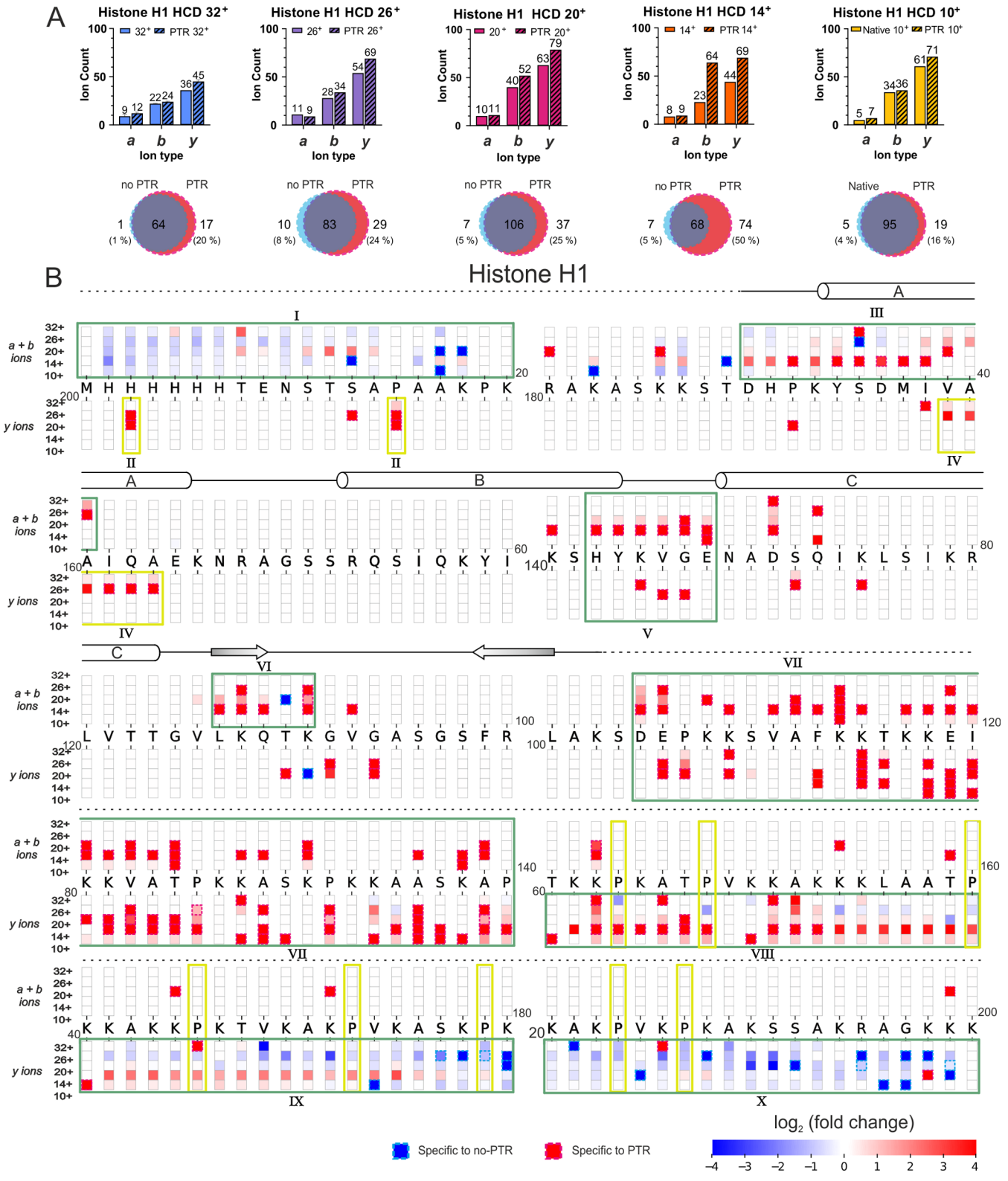


Figure 3. (A) Bar plots show the number of assigned HCD fragment ions from histone H1 for different precursor ion charge states, generated with and without PTR. The Venn diagrams below each bar plot indicate the number of fragment ions unique to each condition. (B) Heatmap of histone H1 showing the $\log_2$ fold change in fragment-ion abundance with and without PTR. The amino acid sequence is shown in the middle, with the protein secondary structure indicated above the heatmap (dashed lines denote regions lacking known defined structure). The squares represent fragment ions observed at each interresidue cleavage site: *a*/*b*-fragment ions are displayed above the sequence; *y*-ions are displayed below the sequence. Each row corresponds to a precursor ion charge state. Red indicates increased fragment ion abundance relative to no PTR. Blue indicates decreased fragment ion abundance relative to noPTR. Fragment ions observed exclusively with or without PTR are outlined with red or blue dashed borders, respectively, as indicated by Venn diagrams.

https://doi.org/10.1021/acs.analchem.6c04013
Anal. Chem. 2026, 98, 29299−29311

Downloaded from pubs.acs.org/ancham/article-pdf/98/40/29299/6868094/acs.analchem.6c04013.pdf by FLORIDA STATE UNIV user on 02 November 2026

states, extensive proton mobility can mask subtle differences in fragmentation behavior, whereas at lower charge states fragmentation becomes increasingly sensitive to differences in charge distribution and regional accessibility within the protein.

The comparison of $^{PTR}8^+$, with its native-like counterpart did not show a substantial increase in fragment ion assignments, which can be explained by a lack of mobile protons at this charge state (Supplemental Figure S8). Despite their similar fragment-ion yields, different fragmentation behavior, specifically cleavages C-terminal to aspartic acids, and substantial quantitative differences indicate altered gas-phase structures.

In the case of apocalmodulin, the fragmentation behavior was markedly different from that observed for apomyoglobin (Figure 2B). The N-terminal loop, helix A, the intervening loop, and helix B exhibited substantial rearrangement with PTR (H4-G60, region I). Specifically, most small *b*-ions disappeared from the spectra following PTR. This loss is also reflected in the Venn diagrams in Figure 2A, which show fewer assigned fragment ions for the $^{PTR}18^+$ and $^{PTR}15^+$ states. Upon further charge reduction to $^{PTR}10^+$ and $^{PTR}8^+$, some of these small *b*-ions reappeared, though at lower abundance than in the no PTR controls. This effect gradually diminishes along helix B and into helix C. The most substantial alterations in fragmentation behavior occurred in helix C and the intervening loop preceding helix D (region II), where numerous newly generated fragment ions were observed across all reduced charge states, along with significantly increased fragment-ion abundance. Although the native-like apocalmodulin also generated fragment ions in this region, PTR clearly induces a distinct structural ensemble with an even greater susceptibility to backbone cleavage. Additional changes were observed in the C-terminal loop near helix H (region III). Here, lower-MW *y*-ions decreased after PTR and several unique *b*-ions appeared in the $^{PTR}18^+$ state. These *b*-ions were observed only at this intermediate charge state and were no longer detected upon further charge reduction, consistent with extensive charge reduction and limited availability of mobile protons in this region.

The opportunity for apocalmodulin to undergo structural rearrangement during PTR may be constrained by the large number of acidic residues and the extensive network of potential salt bridges within the sequence. These interactions can stabilize certain gas-phase conformers and limit the accessibility of backbone sites to fragmentation. This structural rigidity may explain why few new fragment ions are generated in the region spanning helices D-F. Although some fragment ions from these regions were detected, suggesting that persistent intramolecular interactions restrict fragmentation in this part of the protein.

Reducing apocalmodulin to the $^{PTR}8^+$ charge state gave rise to several new fragment ions within region IV. Notably, three unique backbone cleavage sites at residues F88, L89, and T90 were observed, supported by the corresponding fragment ions b_{89}, y_{79}, y_{80}, and y_{81} (region IV, Figure 2B). These ions were absent in the spectrum of native-like apocalmodulin, indicating that extensive charge reduction exposes regions of the sequence that are otherwise protected from fragmentation. Despite the appearance of these new cleavage sites, relatively few fragment ions were generated in the $^{PTR}8^+$ state (Supplemental Figure S8), consistent with the mobile-proton constraints.[35,37,43]

During the PTR process, mobile protons are more likely to undergo reaction than those localized to basic residues. In contrast, localized protons can stabilize the conformation by forming salt bridges ($H^+/K^+/R^+$ with D^-/E^-) and zwitterionic contacts, thereby decreasing their likelihood of participating in proton transfer. Even though the $^{PTR}8^+$ state should retain one mobile proton (8 protons on a molecule bearing 7 arginine residues), fragmentation remains strongly biased toward cleavages C-terminal to aspartic and glutamic acid residues, a well-established observation for low-charge precursor ions under mobile-proton-limited conditions.[35] Similar fragmentation has been reported for the $^{PTR}8^+$ state of apocalmodulin by the Brodbelt group,[37] for low charge states of ubiquitin by the McLuckey group,[54] Furthermore, fixing the charge by covalent probes on basic residues resulted in enhanced protein fragmentation c-terminal to aspartic/glutamic acids.[38] Figure 2B highlights several prominent examples at D113, D115, D138, D142, D150, D152, and D154 that showed abundant, PTR-only induced cleavages on their C-terminal side in low charge states (regions V).

Histone H1

Histone H1 (~22 kDa) is a basic, lysine-rich protein containing 4 × D, 5 × E, 56 × K, and 6 × R residues, (estimated pI ~11.33). This protein functions as part of the nucleosome complex.

Here, histone H1 was evaluated similarly across a series of five targeted ion charge states starting from the $[M + 38H]^{38+}$ precursor: $^{PTR}32^+$, $^{PTR}26^+$, $^{PTR}20^+$, $^{PTR}14^+$, and $^{PTR}10^+$ (Supplemental Figure S9). The $^{PTR}10^+$ charge state was compared to the same charge state generated from native-like conditions. As illustrated in Figure 3A, HCD of charge-reduced precursor ions produced a consistent increase in the number of newly observed fragments as the extent of charge reduction increased from $^{PTR}32^+$ to $^{PTR}14^+$ (17, 29, 37, and 74 for $^{PTR}32^+$, $^{PTR}26^+$ $^{PTR}20^+$, $^{PTR}14^+$, respectively). The highest fragment ion yields were obtained for $^{PTR}20^+$ and $^{PTR}14^+$, with total 142 assigned fragment ions, respectively. Of these, 37 and 74 were uniquely generated after PTR. Similar to apomyoglobin and apocalmodulin, the lowest charge state, $^{PTR}10^+$, exhibited reduced fragment ion yield, consistent with the limited availability of mobile protons and increased gas-phase compaction at low charge states (Supplemental Figure S10). Although only a small number of additional fragment ions were generated from the $^{PTR}10^+$ charge state of histone H1 (19 new fragment ions), they are predominantly located at the C-terminal region, confirming distinct fragmentation behavior compared to histone H1 sprayed from native-like conditions.

Figure 3B displays the heatmap for histone H1. Protein topology denoted with a dashed line in Figure 3B reflects unknown secondary structure,[55] indicating that histone H1 possesses extensive disordered domains. The N-terminal region of histone H1, including its His_6-tag, showed a decrease in abundance of smaller *b*-ions with PTR (region I). This behavior is similar to that observed in the apocalmodulin His_6-tag region. Two notable cleavages N-terminal to H3 and P15 were uniquely observed in the $^{PTR}26^+$ and $^{PTR}20^+$ states as y_{198} and y_{186}, respectively (region II). Another region of interest spans helix A (D30−A41, region III). At higher charge states, smaller *b*-ions show modest changes, but several unique *b*-ions were observed in $^{PTR}14^+$. Additionally, a series of high-MW *y*-ions in helix A, V39-A44 (y_{157}−y_{162}, region IV), was generated at slightly higher abundance in $^{PTR}32^+$ compared to the [M +

Downloaded from pubs.acs.org/ancham/article-pdf/98/40/29299/6680948/acs.analchem.6c04013.pdf by FLORIDA STATE UNIV user on 02 November 2026

https://doi.org/10.1021/acs.analchem.6c04013
Anal. Chem. 2026, 98, 29299−29311

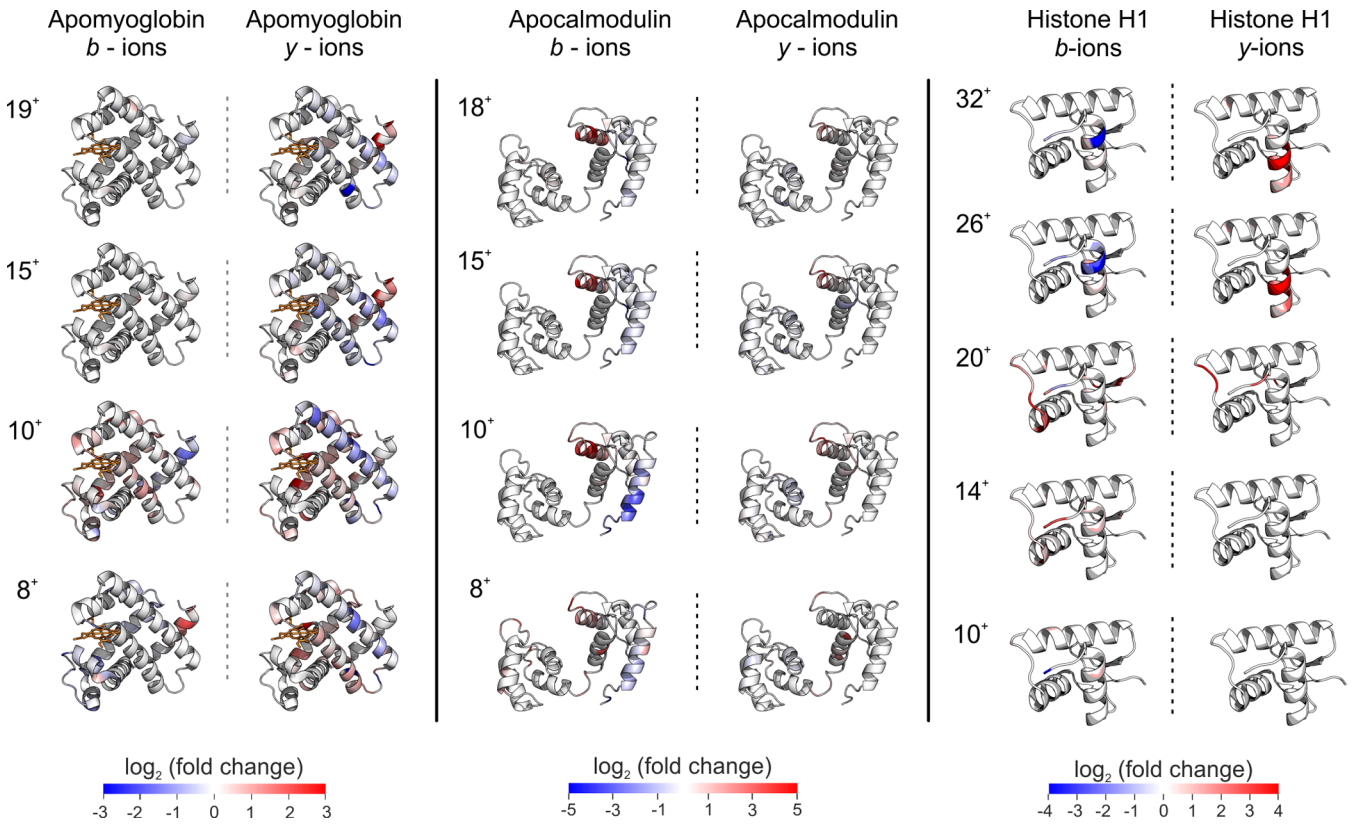


Figure 4. Heatmap based quantitative changes superimposed onto respective models for both *b*- and *y*-ions separately, and for apomyoglobin (PDB entry: 1WLA), apocalmodulin (PDB entry: 1DMO/4), and histone H1 (PDB entry: 7K5X). The models were constructed based on the heatmaps displayed in Figures 1B, 2B and 3B.

$32H]^{32+}$ precursor generated without PTR, and showed a marked increase in abundance in the $^{PTR}26^{+}$ state. One representative ion from this region, y_{159}, is shown in Supplemental Figure S11. Upon fragmentation of the $[M + 32H]^{32+}$ precursor without PTR, the y_{159}^{23+}, y_{159}^{24+} and y_{159}^{25+} -ions were observed and, with PTR, the y_{159}^{23+}- through y_{159}^{26+}-ions fragment ions were detected. For the $[M + 26H]^{26+}$ precursor, y_{159} appeared only with PTR, in the 19^{+}-21^{+} charge states. This fragment was not detected for the 20^{+}, 14^{+}, or 10^{+} precursor ion charge states.

Additional newly generated *b*-ions were detected at the end of helix B and in the intervening loop preceding helix C (H63-E68, region V), as well as in the *β*-sheet region following helix C (L87−K91, region VI). These fragment ions were predominantly generated from lower charge states, consistent with structural rearrangement. The most dramatic increase in unique fragment ions was observed in the region spanning D105−P140 (region VII). This region lacks defined secondary structure and contains 4 proline and 14 lysine residues. Notably, as additional protons were stripped during PTR, an increase in unique *b*- and *y*-ions arose from this region, suggesting this behavior may reflect conformational changes around proline residues——a common feature associated with turns and flexible motifs in native protein folds.

The C-terminal region of histone H1 contains a high density of proline residues. The fragmentation trend of corresponding *y*-ions is similar to those seen for proline residues in apomyoglobin. The most substantial changes occurred in the T141−P160 segment (region VIII), with a strong preference for *y*-ions generated from this region after PTR. The adjacent region spanning K161−K180 (region IX) also displayed clear evidence of structural rearrangement, initially with lower ion abundance with PTR, but the trend is reversed with the progressive PTR, specifically in the $^{PTR}14^{+}$ and $^{PTR}10^{+}$ precursor ions. Lastly, the C-terminal region (K181−K200, region X), dominated by small *y*-ions (y_1−y_{20}), showed a decrease in *y*-ion abundance, which may indicate reduced susceptibility of this region to HCD fragmentation.

Interestingly, throughout this region, *y*-ions bearing N-terminal proline residues (denoted in yellow boxes) were generated to varying extents after PTR. This behavior is particularly intriguing because cleavage N-terminal to proline is generally disfavored in low-charge ions where limited proton mobility restricts the activation of proline-adjacent backbone sites.[54,56] This behavior may reflect PTR-induced changes in proton relocalization and local backbone conformation around proline residues, which can increase the susceptibility of N-terminal to proline cleavages under HCD conditions.

The fragmentation patterns described throughout this work reflect structural protein ion changes that result from gas-phase ion−ion reactions. We have mapped these changes upon the respective PDB X-ray crystal structures for each of the proteins in this study to provide a visual representation of these underlying changes (Figure 4).

The influence of charge on gas-phase ion conformation has also been explored previously, most notably through ion-mobility (IM) experiments. Ion mobility spectrometry provides an exceptional analytical tool which can directly correlate collision cross sections (CCS, Å^2) with charge states.[57,58] An early ion mobility study from Shelimov and coworkers[59] on charge-reduced apomyoglobin shows that higher charge states (11^{+}−22^{+}) possess mostly linear-like

Downloaded from pubs.acs.org/ancham/article-pdf/98/40/29299/6868094/acs.analchem.6c04013.pdf by FLORIDA STATE UNIV user on 02 November 2026

https://doi.org/10.1021/acs.analchem.6c04013
Anal. Chem. 2026, 98, 29299−29311

conformations. Proton stripping into 8^+ resulted in two distinct compact conformers, with one being preferred one. The bimodal distribution can be explained by broadband electrospray-generated reduction; however, this result further confirms that PTR-based ions do possess different conformations. One of the earliest studies also examined cytochrome *c* following charge reduction in a 3D-IT−IM−time-of-flight (TOF) instrument,[60] and showed that charge-reduced ions adopt CCS comparable to those observed when the protein is electrosprayed under native-like conditions, though the charge reduced ions were slightly larger and populated two distinct conformers. When individual charge states were compared, CCS values decreased progressively down to the 5^+ charge state and then increased slightly for lower charge states,[60] suggesting a transition point at which the loss of Coulomb repulsion permits substantial gas-phase compaction. These results correlate with the earlier work from Shelimov and coworkers on cytochrome *c*.[61] A similar trend was reported for ubiquitin,[62] although the differences were less pronounced, presumably due to the absence of structural constraints such as the covalently bound heme group present in cytochrome *c*. Additional IM studies have identified structural differences between ubiquitin ions with and without charge reduction, although some measurements report minimal CCS changes depending on instrumental conditions.[26,37] More pronounced CCS changes have been documented for larger proteins, such as serum albumin,[29] indicating that the magnitude of charge-reduction-induced compaction is protein-dependent. Recent work from the Konermann group[28] using MD simulations has shown that reduced Coulomb repulsion can drive extensive rearrangements that yield compact structures with CCS values similar to native-like ions while adopting markedly different topologies. Because these rearrangements are driven by localized electrostatic interactions, the overall size of reduced ions is expected to approximate native-like dimensions, while the extent and location of structural reorganization remain sequence-dependent, particularly in proteins capable of forming extensive networks of salt bridges. Nevertheless, experiments that utilize chemical probes influencing charge localization or protein basicity[38,63−67] result in altered fragmentation patterns.

CONCLUSION

Proton-transfer reactions provide a powerful means of probing gas-phase protein structure by altering charge distribution and enabling systematic comparison of precursor ions generated directly by electrospray with those produced through controlled charge reduction. Across three model proteins——apomyoglobin, apocalmodulin, and histone H1—we observed that stepwise charge reduction induces gas-phase rearrangement, resulting in regions with increased or decreased susceptibility to backbone cleavage. Moderate charge reduction generally improved sequence information, while extensive charge reduction can decrease fragmentation efficiency through loss of mobile protons and extensive gas-phase collapse, but this effect is dependent upon protein sequence.

The rearrangement process during charge reduction is stochastic and likely leads to a multitude of gas-phase structures. These structures differ compared to their ESI-generated noncharge reduced counterparts, including the ones sprayed from a native-like environment. The latter effect was specifically observed by studying apocalmodulin and histone H1, for which prominent cleavages C-terminal to aspartic acid or N-terminal to proline were observed. Although these preferred cleavage sites may decrease sequence coverage, the rapid gas-phase rearrangement allows fragment ions to be generated from specific protein conformers which are not generated without PTR.

From a practical standpoint, through careful selection of precursor ion charge and extent of charge reduction, improvements and even targeting of regions of greatest sequence coverage may be achieved. Controlled charge reduction can be particularly valuable for targeted top-down sequencing of proteoforms. Moreover, this approach may be helpful in sequencing of specific protein regions to differentiate multiple PTMs,[64,66] especially in regions which are recalcitrant to fragmentation under normal conditions.

ASSOCIATED CONTENT

Data Availability Statement

Supporting Information is available free of charge on the ACS Publications Web site. The data set is publicly available on the Open Science Framework (OSF): 10.17605/OSF.IO/S4K26

Supporting Information

The Supporting Information is available free of charge at https://pubs.acs.org/doi/10.1021/acs.analchem.6c04013.

Figure S1: Log_2FC map of fragment ions for apomyoglobin, apocalmodulin, and histone H1; Figure S2: ESI spectra of apomyoglobin from PTR at different reaction times; Figure S3: sequence coverage of native-like apomyoglobin (8^+) and $^{PTR}8^+$; Figure S4: Bar plot for assigned fragment ions upon fragmenting apomyoglobin with ETD; Figure S5: bar plot for assigned fragment ions upon fragmenting apomyoglobin with CID 10 ms and CID 1 ms; Figure S6: inset HCD spectra of apomyoglobin b_{71} fragment ions, with and without PTR; Figure S7: ESI spectra of apocalmodulin from PTR at different reaction times; Figure S8: sequence coverage of native-like apocalmodulin (8^+) and $^{PTR}8^+$; Figure S9: ESI spectra from histone H1 with PTR at different reaction times; Figure S10: sequence coverage of native-like apocalmodulin (8^+) and $^{PTR}8^+$; Figure S11: Inset HCD spectra of histone H1 y_{159} fragment ion. Table S1: reaction times and energies used in experiments in this study (PDF)

AUTHOR INFORMATION

Corresponding Author

Chad R. Weisbrod − *National High Magnetic Field Laboratory, Tallahassee, Florida 32310, United States;* orcid.org/0000-0001-5324-4525; Email: weisbrod@magnet.fsu.edu

Authors

Marek Polák − *National High Magnetic Field Laboratory, Tallahassee, Florida 32310, United States;* orcid.org/0000-0002-8929-5479

Lissa C. Anderson − *National High Magnetic Field Laboratory, Tallahassee, Florida 32310, United States; Department of Chemistry and Biochemistry, Florida State University, Tallahassee, Florida 32306, United States;* orcid.org/0000-0001-8633-0251

Kristina Håkansson − *National High Magnetic Field Laboratory, Tallahassee, Florida 32310, United States;*

Downloaded from pubs.acs.org/ancham/article-pdf/98/40/29299/6880948/acs.analchem.6c04013.pdf by FLORIDA STATE UNIV user on 02 November 2026

Department of Chemistry and Biochemistry, Florida State University, Tallahassee, Florida 32306, United States; orcid.org/0000-0003-1926-0542

Christopher L. Hendrickson − *National High Magnetic Field Laboratory, Tallahassee, Florida 32310, United States;* orcid.org/0000-0002-4272-2939

Complete contact information is available at: https://pubs.acs.org/10.1021/acs.analchem.6c04013

Author Contributions

The manuscript was written with contributions of all authors. All authors have approved the final version of the manuscript.

Notes

The authors declare no competing financial interest.

■ ACKNOWLEDGMENTS

A portion of this work was performed at the National High Magnetic Field Laboratory, which is supported by the National Science Foundation Divisions of Chemistry and Materials Research through Cooperative Agreement No. DMR-2128556 and the State of Florida. Portions of the manuscript text were drafted or refined with the assistance of AI-based language tools (e.g., ChatGPT, OpenAI), under the direct supervision and final review of the authors.

■ REFERENCES

(1) Konermann, L.; Vahidi, S.; Sowole, M. A. Mass Spectrometry Methods for Studying Structure and Dynamics of Biological Macromolecules. *Anal. Chem.* **2014**, *86* (1), 213−232.

(2) Liu, X. R.; Zhang, M. M.; Gross, M. L. Mass Spectrometry-Based Protein Footprinting for Higher-Order Structure Analysis: Fundamentals and Applications. *Chem. Rev.* **2020**, *120* (10), 4355−4454.

(3) Masson, G. R.; Burke, J. E.; Ahn, N. G.; Anand, G. S.; Borchers, C.; Brier, S.; Bou-Assaf, G. M.; Engen, J. R.; Englander, S. W.; Faber, J.; Garlish, R.; Griffin, P. R.; Gross, M. L.; Guttman, M.; Hamuro, Y.; Heck, A. J. R.; Houde, D.; Iacob, R. E.; Jørgensen, T. J. D.; Kaltashov, I. A.; Klinman, J. P.; Konermann, L.; Man, P.; Mayne, L.; Pascal, B. D.; Reichmann, D.; Skehel, M.; Snijder, J.; Strutzenberg, T. S.; Underbakke, E. S.; Wagner, C.; Wales, T. E.; Walters, B. T.; Weis, D. D.; Wilson, D. J.; Wintrode, P. L.; Zhang, Z.; Zheng, J.; Schriemer, D. C.; Rand, K. D. Recommendations for Performing, Interpreting and Reporting Hydrogen Deuterium Exchange Mass Spectrometry (HDX-MS) Experiments. *Nat. Methods* **2019**, *16* (7), 595−602.

(4) Leitner, A. Cross-Linking and Other Structural Proteomics Techniques: How Chemistry Is Enabling Mass Spectrometry Applications in Structural Biology. *Chem. Sci.* **2016**, *7* (8), 4792−4803.

(5) Britt, H. M.; Cragnolini, T.; Thalassinos, K. Integration of Mass Spectrometry Data for Structural Biology. *Chem. Rev.* **2022**, *122* (8), 7952−7986.

(6) Veale, C. G. L.; Clarke, D. J. Mass spectrometry-based methods for characterizing transient protein−protein interactions. *Trends In Chemistry. Cell* **2024**, *6*, 377−391.

(7) Beckman, J. S.; Voinov, V. G.; Hare, M.; Sturgeon, D.; Vasil'ev, Y.; Oppenheimer, D.; Shaw, J. B.; Wu, S.; Glaskin, R.; Klein, C.; Schwarzer, C.; Stafford, G. Improved Protein and PTM Characterization with a Practical Electron-Based Fragmentation on Q-TOF Instruments. *J. Am. Soc. Mass Spectrom.* **2021**, *32* (8), 2081−2091.

(8) Hunt, D. F.; Shabanowitz, J.; Yates, J. R.; Griffin, P. R.; Zhu, N. Z. Tamdem Quadrupole Fourier Transform Mass Spectrometry. *Anal. Chim. Acta* **1989**, *225* (C), 1−10.

(9) Hunt, D. F.; Shabanowitz, J.; Yates, J. R. Peptide Sequence Analysis by Laser Photodissociation Fourier Transform Mass Spectrometry. *J. Chem. Soc., Chem. Commun.* **1987**, No. 8, 548−550.

(10) Shaw, J. B.; Li, W.; Holden, D. D.; Zhang, Y.; Griep-Raming, J.; Fellers, R. T.; Early, B. P.; Thomas, P. M.; Kelleher, N. L.; Brodbelt, J. S. Complete Protein Characterization Using Top-down Mass Spectrometry and Ultraviolet Photodissociation. *J. Am. Chem. Soc.* **2013**, *135* (34), 12646−12651.

(11) Chi, A.; Huttenhower, C.; Geer, L. Y.; Coon, J. J.; Syka, J. E. P.; Bai, D. L.; Shabanowitz, J.; Burke, D. J.; Troyanskaya, O. G.; Hunt, D. F. Analysis of Phosphorylation Sites on Proteins from Saccharomyces Cerevisiae by Electron Transfer Dissociation (ETD) Mass Spectrometry. *Proc. Natl. Acad. Sci. U. S. A.* **2007**, *104* (7), 2193−2198.

(12) Swaney, D. L.; McAlister, G. C.; Wirtala, M.; Schwartz, J. C.; Syka, J. E. P.; Coon, J. J. Supplemental Activation Method for High-Efficiency Electron-Transfer Dissociation of Doubly Protonated Peptide Precursors. *Anal. Chem.* **2007**, *79* (2), 477−485.

(13) Riley, N. M.; Westphall, M. S.; Coon, J. J. Activated Ion-Electron Transfer Dissociation Enables Comprehensive Top-Down Protein Fragmentation. *J. Proteome Res.* **2017**, *16* (7), 2653−2659.

(14) Youssef, M. M.; Szot, C. W.; Folz, J.; Collier, L. M.; Kweon, H. K.; De Figlia, S. A.; Ayad, M. F.; Hussein, L. A.; Abdel-Ghany, M. F.; Hakansson, K. Electron Capture vs Transfer Dissociation for Site Determination of Tryptic Peptide Tyrosine Sulfation: Direct Detection of Fibrinogen Sulfation Sites and Identification of Novel Isobaric Interferences. *J. Proteome Res.* **2024**, *23* (7), 2386−2396.

(15) Marshall, A. G.; Senko, M. W.; Li, W.; Li, M.; Dillon, S.; Guan, S.; Logan, T. M. Protein Molecular Mass to 1 Da by 13C, 15N Double-Depletion and FT-ICR Mass Spectrometry. *J. Am. Chem. Soc.* **1997**, *119* (2), 433−434.

(16) Gallagher, K. J.; Palasser, M.; Hughes, S.; Mackay, C. L.; Kilgour, D. P. A.; Clarke, D. J. Isotope Depletion Mass Spectrometry (ID-MS) for Accurate Mass Determination and Improved Top-Down Sequence Coverage of Intact Proteins. *J. Am. Soc. Mass Spectrom.* **2020**, *31* (3), 700−710.

(17) Stephenson, J. L.; McLuckey, S. A. Ion/Ion Reactions in the Gas Phase: Proton Transfer Reactions Involving Multiply-Charged Proteins. *J. Am. Chem. Soc.* **1996**, *118* (31), 7390−7397.

(18) Stephenson, J. L.; McLuckey, S. A. Ion/Ion Proton Transfer Reactions for Protein Mixture Analysis. *Anal. Chem.* **1996**, *68* (22), 4026−4032.

(19) McLuckey, S. A.; Stephenson, J. L.; Asano, K. G. Ion/Ion Proton-Transfer Kinetics: Implications for Analysis of Ions Derived from Electrospray of Protein Mixtures. *Anal. Chem.* **1998**, *70* (6), 1198−1202.

(20) Stephenson, J. L.; McLuckey, S. A. Simplification of Product Ion Spectra Derived from Multiply Charged Parent Ions via Ion/Ion Chemistry. *Anal. Chem.* **1998**, *70* (17), 3533−3544.

(21) Chrisman, P. A.; Pitteri, S. J.; McLuckey, S. A. Parallel Ion Parking of Protein Mixtures. *Anal. Chem.* **2006**, *78* (1), 310−316.

(22) Chrisman, P. A.; Pitteri, S. J.; McLuckey, S. A. Parallel Ion Parking: Improving Conversion of Parents to First-Generation Products in Electron Transfer Dissociation. *Anal. Chem.* **2005**, *77* (10), 3411−3414.

(23) Weisbrod, C. R.; Anderson, L. C.; Hendrickson, C. L.; Schaffer, L. V.; Shortreed, M. R.; Smith, L. M.; Shabanowitz, J.; Hunt, D. F. Advanced Strategies for Proton-Transfer Reactions Coupled with Parallel Ion Parking on a 21 T FT-ICR MS for Intact Protein Analysis. *Anal. Chem.* **2021**, *93* (26), 9119−9128.

(24) Ugrin, S. A.; English, A. M.; Syka, J. E. P.; Bai, D. L.; Anderson, L. C.; Shabanowitz, J.; Hunt, D. F. Ion-Ion Proton Transfer and Parallel Ion Parking for the Analysis of Mixtures of Intact Proteins on a Modified Orbitrap Mass Analyzer. *J. Am. Soc. Mass Spectrom.* **2019**, *30* (10), 2163−2173.

(25) Duselis, E. M.; Panepinto, M. C.; Syka, J. E. P.; Mullen, C.; D'ippolito, R. A.; English, A. M.; Ugrin, S. A.; Shabanowitz, J.; Hunt, D. F. Improved Sequence Analysis of Intact Proteins by Parallel Ion Parking during Electron Transfer Dissociation. *Anal. Chem.* **2021**, *93* (47), 15728−15735.

(26) Laszlo, K. J.; Munger, E. B.; Bush, M. F. Folding of Protein Ions in the Gas Phase after Cation-to-Anion Proton-Transfer Reactions. *J. Am. Chem. Soc.* **2016**, *138* (30), 9581−9588.

Downloaded from pubs.acs.org/ancham/article-pdf/98/40/29299/6868094/acs.analchem.6c04013.pdf by FLORIDA STATE UNIV user on 02 November 2026

(27) Butcher, D.; Miksovska, J.; Ridgeway, M. E.; Park, M. A.; Fernandez-Lima, F. The Effects of Solution Additives and Gas-phase Modifiers on the Molecular Environment and Conformational Space of Common Heme Proteins. *Rapid Commun. Mass Spectrom.* **2019**, *33* (5), 399−404.
(28) Sever, A. I. M.; Konermann, L. Gas Phase Protein Folding Triggered by Proton Stripping Generates Inside-Out Structures: A Molecular Dynamics Simulation Study. *J. Phys. Chem. B* **2020**, *124* (18), 3667−3677.
(29) Gadzuk-Shea, M. M.; Bush, M. F. Effects of Charge State on the Structures of Serum Albumin Ions in the Gas Phase: Insights from Cation-to-Anion Proton-Transfer Reactions, Ion Mobility, and Mass Spectrometry. *J. Phys. Chem. B* **2018**, *122* (43), 9947−9955.
(30) Gandhi, V. D.; Hua, L.; Lawrenz, M.; Latif, M.; Rolland, A. D.; Campuzano, I. D. G.; Larriba-Andaluz, C. Elucidating Protein Structures in the Gas Phase: Traversing Configuration Space with Biasing Methods. *J. Chem. Theory Comput.* **2024**, *20* (21), 9720−9733.
(31) Senko, M. W.; Remes, P. M.; Canterbury, J. D.; Mathur, R.; Song, Q.; Eliuk, S. M.; Mullen, C.; Earley, L.; Hardman, M.; Blethrow, J. D.; Bui, H.; Specht, A.; Lange, O.; Denisov, E.; Makarov, A.; Horning, S.; Zabrouskov, V. Novel Parallelized Quadrupole/Linear Ion Trap/Orbitrap Tribrid Mass Spectrometer Improving Proteome Coverage and Peptide Identification Rates. *Anal. Chem.* **2013**, *85* (24), 11710−11714.
(32) Kline, J. T.; Mullen, C.; Durbin, K. R.; Oates, R. N.; Huguet, R.; Syka, J. E. P.; Fornelli, L. Sequential Ion-Ion Reactions for Enhanced Gas-Phase Sequencing of Large Intact Proteins in a Tribrid Orbitrap Mass Spectrometer. *J. Am. Soc. Mass Spectrom.* **2021**, *32* (9), 2334−2345.
(33) Oates, R. N.; Lieu, L. B.; Kline, J. T.; Mullen, C.; Srzentić, K.; Huguet, R.; McAlister, G. C.; Huang, J.; Bergen, D.; Melani, R. D.; Zabrouskov, V.; Durbin, K. R.; Syka, J. E. P.; Fornelli, L. Towards a Universal Method for Middle-down Analysis of Antibodies via Proton Transfer Charge Reduction—Orbitrap Mass Spectrometry. *Anal. Bioanal. Chem.* **2024**, *416* (28), 6463−6472.
(34) Lieu, L. B.; Nagy, C.; Huang, J.; Mullen, C.; McAlister, G. C.; Zabrouskov, V.; Srzentić, K.; Durbin, K. R.; Melani, R. D.; Fornelli, L. Enhanced Payload Localization in Antibody-Drug Conjugates Using a Middle-Down Mass Spectrometry Approach with Proton Transfer Charge Reduction. *Anal. Chem.* **2024**, *96* (46), 18483−18490.
(35) Wysocki, V. H.; Tsaprailis, G.; Smith, L. L.; Breci, L. A. Mobile and Localized Protons: A Framework for Understanding Peptide Dissociation. *J. Mass Spectrom.* **2000**, *35* (12), 1399−1406.
(36) Haverland, N. A.; Skinner, O. S.; Fellers, R. T.; Tariq, A. A.; Early, B. P.; Le Duc, R. D.; Fornelli, L.; Compton, P. D.; Kelleher, N. L. Defining Gas-Phase Fragmentation Propensities of Intact Proteins During Native Top-Down Mass Spectrometry. *J. Am. Soc. Mass Spectrom.* **2017**, *28* (6), 1203−1215.
(37) Bashyal, A.; Sanders, J. D.; Holden, D. D.; Brodbelt, J. S. Top-Down Analysis of Proteins in Low Charge States. *J. Am. Soc. Mass Spectrom.* **2019**, *30* (4), 704−717.
(38) Polasky, D. A.; Dixit, S. M.; Keating, M. F.; Gadkari, V. V.; Andrews, P. C.; Ruotolo, B. T. Pervasive Charge Solvation Permeates Native-like Protein Ions and Dramatically Influences Top-down Sequencing Data. *J. Am. Chem. Soc.* **2020**, *142* (14), 6750−6760.
(39) Syka, J. E. P.; Coon, J. J.; Schroeder, M. J.; Shabanowitz, J.; Hunt, D. F. Peptide and Protein Sequence Analysis by Electron Transfer Dissociation Mass Spectrometry. *Proc. Natl. Acad. Sci. U. S. A.* **2004**, *101* (26), 9528−9533.
(40) Kjeldsen, F.; Haselmann, K. F.; Budnik, B. A.; Jensen, F.; Zubarev, R. A. Dissociative Capture of Hot (3−13 EV) Electrons by Polypeptide Polycations: An Efficient Process Accompanied by Secondary Fragmentation. *Chem. Phys. Lett.* **2002**, *356* (3−4), 201−206.
(41) Breuker, K.; Oh, H. B.; Horn, D. M.; Cerda, B. A.; McLafferty, F. W. Detailed Unfolding and Folding of Gaseous Ubiquitin Ions Characterized by Electron Capture Dissociation. *J. Am. Chem. Soc.* **2002**, *124* (22), 6407−6420.
(42) Skinner, O. S.; McAnally, M. O.; Van Duyne, R. P.; Schatz, G. C.; Breuker, K.; Compton, P. D.; Kelleher, N. L. Native Electron Capture Dissociation Maps to Iron-Binding Channels in Horse Spleen Ferritin. *Anal. Chem.* **2017**, *89* (20), 10711−10716.
(43) Vorobyev, A.; Hamidane, H. B.; Tsybin, Y. O. Electron Capture Dissociation Product Ion Abundances at the X Amino Acid in RAAAA-X-AAAAK Peptides Correlate with Amino Acid Polarity and Radical Stability. *J. Am. Soc. Mass Spectrom.* **2009**, *20* (12), 2273−2283.
(44) Savitski, M. M.; Kjeldsen, F.; Nielsen, M. L.; Zubarev, R. A. Hydrogen Rearrangement to and from Radical z Fragments in Electron Capture Dissociation of Peptides. *J. Am. Soc. Mass Spectrom.* **2007**, *18* (1), 113−120.
(45) Zubarev, R. A.; Zubarev, A. R.; Savitski, M. M. Electron Capture/Transfer versus Collisionally Activated/Induced Dissociations: Solo or Duet? *J. Am. Soc. Mass Spectrom.* **2008**, *19* (6), 753−761.
(46) Li, W.; Song, C.; Bailey, D. J.; Tseng, G. C.; Coon, J. J.; Wysocki, V. H. Statistical Analysis of Electron Transfer Dissociation Pairwise Fragmentation Patterns. *Anal. Chem.* **2011**, *83* (24), 9540−9545.
(47) De Graaf, E. L.; Altelaar, A. F. M.; Van Breukelen, B.; Mohammed, S.; Heck, A. J. R. Improving SRM Assay Development: A Global Comparison between Triple Quadrupole, Ion Trap, and Higher Energy CID Peptide Fragmentation Spectra. *J. Proteome Res.* **2011**, *10* (9), 4334−4341.
(48) Xia, Y.; Liang, X.; McLuckey, S. A. Ion Trap versus Low-Energy Beam-Type Collision-Induced Dissociation of Protonated Ubiquitin Ions. *Anal. Chem.* **2006**, *78* (4), 1218−1227.
(49) Hopper, J. T. S.; Oldham, N. J. Collision Induced Unfolding of Protein Ions in the Gas Phase Studied by Ion Mobility-Mass Spectrometry: The Effect of Ligand Binding on Conformational Stability. *J. Am. Soc. Mass Spectrom.* **2009**, *20* (10), 1851−1858.
(50) Pierson, N. A.; Clemmer, D. E. An IMS−IMS Threshold Method for Semi-Quantitative Determination of Activation Barriers: Interconversion of Proline Cis↔trans Forms in Triply Protonated Bradykinin. *Int. J. Mass Spectrom.* **2015**, *377* (1), 646−654.
(51) Popa, V.; Trecroce, D. A.; McAllister, R. G.; Konermann, L. Collision-Induced Dissociation of Electrosprayed Protein Complexes: An All-Atom Molecular Dynamics Model with Mobile Protons. *J. Phys. Chem. B* **2016**, *120* (23), 5114−5124.
(52) Silzel, J. W.; Murphree, T. A.; Paranji, R. K.; Guttman, M. M.; Julian, R. R. Probing the Stability of Proline Cis/Trans Isomers in the Gas Phase with Ultraviolet Photodissociation. *J. Am. Soc. Mass Spectrom.* **2020**, *31* (9), 1974−1980.
(53) Boyd, R.; Somogyi, Á. The Mobile Proton Hypothesis in Fragmentation of Protonated Peptides: A Perspective. *J. Am. Soc. Mass Spectrom.* **2010**, *21* (8), 1275−1278.
(54) Reid, G. E.; Wu, J.; Chrisman, P. A.; Wells, J. M.; McLuckey, S. A. Charge-State-Dependent Sequence Analysis of Protonated Ubiquitin Ions via Ion Trap Tandem Mass Spectrometry. *Anal. Chem.* **2001**, *73* (14), 3274−3281.
(55) Zhou, B. R.; Feng, H.; Kale, S.; Fox, T.; Khant, H.; de Val, N.; Ghirlando, R.; Panchenko, A. R.; Bai, Y. Distinct Structures and Dynamics of Chromatosomes with Different Human Linker Histone Isoforms. *Mol. Cell* **2021**, *81* (1), 166−182.e6.
(56) Breci, L. A.; Tabb, D. L.; Yates, J. R.; Wysocki, V. H. Cleavage N-Terminal to Proline: Analysis of a Database of Peptide Tandem Mass Spectra. *Anal. Chem.* **2003**, *75* (9), 1963−1971.
(57) Kafader, J. O.; Melani, R. D.; Schachner, L. F.; Ives, A. N.; Patrie, S. M.; Kelleher, N. L.; Compton, P. D. Native vs Denatured: An in Depth Investigation of Charge State and Isotope Distributions. *J. Am. Soc. Mass Spectrom.* **2020**, *31* (3), 574−581.
(58) Bush, M. F.; Hall, Z.; Giles, K.; Hoyes, J.; Robinson, C. V.; Ruotolo, B. T. Collision Cross Sections of Proteins and Their Complexes: A Calibration Framework and Database for Gas-Phase Structural Biology. *Anal. Chem.* **2010**, *82* (22), 9557−9565.
(59) Shelimov, K. B.; Jarrold, M. F. Conformations, Unfolding, and Refolding of Apomyoglobin in Vacuum: An Activation Barrier for

Downloaded from pubs.acs.org/ancham/article-pdf/98/40/29299/6880948/acs.analchem.6c04013.pdf by FLORIDA STATE UNIV user on 02 November 2026

https://doi.org/10.1021/acs.analchem.6c04013
Anal. Chem. 2026, 98, 29299−29311

Gas-Phase Protein Folding. *J. Am. Chem. Soc.* **1997**, *119* (13), 2987−2994.
(60) Zhao, Q.; Schieffer, G. M.; Soyk, M. W.; Anderson, T. J.; Houk, R. S.; Badman, E. R. Effects of Ion/Ion Proton Transfer Reactions on Conformation of Gas-Phase Cytochrome c Ions. *J. Am. Soc. Mass Spectrom.* **2010**, *21* (7), 1208−1217.
(61) Shelimov, K. B.; Clemmer, D. E.; Hudgins, R. R.; Jarrold, M. F. Protein Structure in Vacuo: Gas-Phase Conformations of BPTI and Cytochrome C. *J. Am. Chem. Soc.* **1997**, *119* (9), 2240−2248.
(62) Zhao, Q.; Soyk, M. W.; Schieffer, G. M.; Fuhrer, K.; Gonin, M. M.; Houk, R. S.; Badman, E. R. An Ion Trap-Ion Mobility-Time of Flight Mass Spectrometer with Three Ion Sources for Ion/Ion Reactions. *J. Am. Soc. Mass Spectrom.* **2009**, *20* (8), 1549−1561.
(63) Polasky, D. A.; Lermyte, F.; Nshanian, M.; Sobott, F.; Andrews, P. C.; Loo, J. A.; Ruotolo, B. T. Fixed-Charge Trimethyl Pyrilium Modification for Enabling Enhanced Top-Down Mass Spectrometry Sequencing of Intact Protein Complexes. *Anal. Chem.* **2018**, *90* (4), 2756−2764.
(64) Krusemark, C. J.; Frey, B. L.; Belshaw, P. J.; Smith, L. M. Modifying the Charge State Distribution of Proteins in Electrospray Ionization Mass Spectrometry by Chemical Derivatization. *J. Am. Soc. Mass Spectrom.* **2009**, *20* (9), 1617−1625.
(65) Anderson, L. C.; English, A. M.; Wang, W.-H.; Bai, D. L.; Shabanowitz, J.; Hunt, D. F. Protein Derivatization and Sequential Ion/Ion Reactions to Enhance Sequence Coverage Produced by Electron Transfer Dissociation Mass Spectrometry. *Int. J. Mass Spectrom.* **2015**, *377* (1), 617−624.
(66) Abelin, J. G.; Trantham, P. D.; Penny, S. A.; Patterson, A. M.; Ward, S. T.; Hildebrand, W. H.; Cobbold, M.; Bai, D. L.; Shabanowitz, J.; Hunt, D. F. Complementary IMAC Enrichment Methods for HLA-Associated Phosphopeptide Identification by Mass Spectrometry. *Nat. Protoc.* **2015**, *10* (9), 1308−1318.
(67) He, L.; Purcell, A. G.; Beran, G. J. O.; Zhu, Y.; Coronado, K. R.; Mann, S. I.; Harman, W. H.; Julian, R. R. Radical-Initiated Photodissociation at Tryptophan Residues within Intact Proteins in the Gas Phase. *J. Am. Chem. Soc.* **2025**, *147* (32), 28583−28588.

Downloaded from pubs.acs.org/ancham/article-pdf/98/40/29299/6880948/acs.analchem.6c04013.pdf by FLORIDA STATE UNIV user on 02 November 2026

https://doi.org/10.1021/acs.analchem.6c04013
Anal. Chem. 2026, 98, 29299−29311